RSC Advances

PAPER



Cite this: *RSC Adv.*, 2023, **13**, 12469

# Isomerization and reaction process of $N_2O_4(H_2O)_n$

Yi Guo,[a] Zhiyong Huang,[a] Gan Tian,[a] Wei Wu,[b] Jie Lin[c] and Xinlong Chang*[a]

Received 7th March 2023
Accepted 3rd April 2023

DOI: 10.1039/d3ra01515g

rsc.li/rsc-advances

Liquid propellant $N_2O_4$ is prone to absorb $H_2O$ to form an $N_2O_4(H_2O)_n$ system during long-term storage, ultimately generating $HNO_3$, $HNO_2$, and other substances capable of corroding the storage tank, which will adversely affect the performance of weapons and equipment. In this work, the reaction process of the $N_2O_4(H_2O)_n$ system is simulated using density functional theory, and the potential energy surface, the geometric configurations of the molecules, the charge distribution, and the bond parameters of the reaction course at $n = 0$–3 are analyzed. The results show that the potential energy of the system is lower and the structure is more stable when the $H_2O$ in the $N_2O_4(H_2O)_n$ system is distributed on the same side. When $n = 1$ or 2, the reaction profiles are similar, and the systems are partly ionic, although still mainly covalently bonded. When $n = 3$, the charge on the *trans*-$ONONO_2$ group and the $ON–ONO_2$ bond length change abruptly to −0.503 a.u. and 2.57 Å, respectively, at which point the system is dominated by ionic bonds. At $n = 2$, a proton-transfer phenomenon occurs in the reaction course, with partial reverse charge-transfer from $NO_3^-$ to $NO^+$, making the $ON–ONO_2$ bond less susceptible to cleavage, further verifying that $N_2O_4(H_2O)_n$ tends to afford the products directly in one step as $H_2O$ accumulates in the system.

## 1 Introduction

Liquid-fuelled strategic missiles mainly use $N_2O_4$ and unsym-dimethylhydrazine (UDMH) as propellants, and during long-term storage, $N_2O_4$ as an oxidant will absorb moisture from the surrounding environment to produce an $N_2O_4(H_2O)_n$ system, ultimately generating $HNO_3$, $HNO_2$, and other corrosive substances, accelerating corrosion of the receptacle and potentially allowing propellants to leak.[1] Traditional liquid-fuelled strategic missiles are constrained by this factor and can only be temporarily refilled with $N_2O_4$ before launch to shorten the contact time between $N_2O_4$ and the receptacle, but this process leads to long preparation cycles and slow operational response of such missiles, to the detriment of their operational performance.

$N_2O_4$ is a volatile, reddish-brown transparent liquid at room temperature. It is a highly toxic chemical, which hampers experimental studies. $N_2O_4$, as a dimer of $NO_2$, is an important intermediate (IM) in the hydrolysis of $NO_2$ and plays an important role in the formation of acid rain.[2] Due to its noxious nature, the use of quantum calculations to probe the evolution of the $N_2O_4(H_2O)_n$ system is a trend of current research. Some studies have been carried out on the isomerization and self-ionization of $N_2O_4$ and the dimerization of $NO_2$, but the understanding of the chemical mechanism is still incomplete.[3–14] In particular, the effect of $H_2O$ on the $N_2O_4(H_2O)_n$ system needs to be explored more deeply. Pimentel *et al.*[5] found that $N_2O_4$ isomerization and $NO_2$ dimerization in the presence of $H_2O$ can directly form $ONO–NO_2$. Miller *et al.*[4] simulated the interaction of $H_2O$ with $ONO–NO_2$ at room temperature. For the $N_2O_4(H_2O)_n$ system, the ionization rate is two orders of magnitude lower when $n = 1$ and 2 than when $n > 2$, indicating that, in the latter case, the reaction is transient and there is no IM. Medeiros *et al.*[6] mentioned that local minima for the $N_2O_4(H_2O)_n$ system can only be found when $n$ is odd. Putikam *et al.*[9] found a "roaming-like" transition state f formed in $ONO–NO_2$ during the collision with $H_2O$ by the stretching of the N–N bond and the rotation of the $–NO_2$ group. Finlayson-Pitts *et al.*[10] proposed a mechanism for the hydrolysis of $N_2O_4$:

$$2NO_2(g) \leftrightarrow N_2O_4(g) \quad (1)$$

$$N_2O_4(g) \leftrightarrow N_2O_4(surface) \quad (2)$$

$$N_2O_4(surface) \rightarrow ONONO_2(surface) \quad (3)$$

$$ONONO_2(surface) \rightarrow NO^+NO_3^-(surface) \quad (4)$$

$$NO^+NO_3^-(surface) + H_2O \rightarrow HONO(g) + HNO_3(surface) \quad (5)$$

$N_2O_4$ first forms *sym*-$N_2O_4$, which isomerizes to $ONO–NO_2$ and then reacts with $H_2O$ to form HONO and $HNO_3$. The above hydrolysis mechanism reveals the complex diversity of species in the $N_2O_4(H_2O)_n$ system and the high number of isomers of

[a]School of Missile Engineering, Rocket Force University of Engineering, Xi'an, 710025, China. E-mail: xinlongch@vip.sina.com

[b]Center of Engineering Quality Supervision, Logistics Support Department, Beijing, 100142, China

[c]School of Electronic Information and Communication, Huazhong University of Science and Technology, Wuhan, 430074, China

$N_2O_4$.[3] The precise structures of the resulting HONO and $HNO_3$ after combining with $H_2O$ remain uncertain.

In the propellant storage environment, $N_2O_4$ is distinct from that in the atmospheric environment and exists mainly in liquid form. The reaction profile of the $N_2O_4(H_2O)_n$ system after absorbing $H_2O$ from air and forming the $N_2O_4(H_2O)_n$ system is unclear. Therefore, in this study, we have investigated the isomerization and reaction profile of the $N_2O_4(H_2O)_n$ system based on density functional theory (DFT), focusing on the following issues:

(1) The effects on the $N_2O_4(H_2O)_n$ system of $n$ being an odd or even number.

(2) The route by which the $N_2O_4(H_2O)_n$ system directly forms $NO^+$ and $NO_3^-$.

(3) The variations in the charges on the groups during the reaction course of the $N_2O_4(H_2O)_n$ system when $n = 0$–3.

## 2 Calculation method

Based on the conclusions of Pimentel *et al.*,[5] the DFT/B3LYP method was used to optimize $N_2O_4$ single-molecule isomerization at the 6-311++G (3df, 2p) basis group level, considering all species in the reaction of the $N_2O_4(H_2O)_n$ system. The intrinsic reaction coordinates (IRC) were established through standard 6-311++G (3df, 2p) basis group calculations to confirm the connection of each transition state (TS) to the specified intermediate (IM). The resulting reactant, product, and IM frequencies were positive, with one and only one imaginary frequency for the TS. Single-point energies were re-determined at the B2PLYP/Def2-TZVP basis set level.[15] To take into account the effect of the solvent medium, the self-consistent reaction field (SCRF) method and the implicit solvation model of the SMD model were used at $n = 3$, in conjunction with the conclusions of Miller[4] and Putikam.[9] All calculations were performed using the Gaussian 16 software package.[16]

## 3 Results and discussion

### 3.1 Isomerization of $N_2O_4$ ($n = 0$)

Experimental studies have shown that $N_2O_4$ has three main conformations; in addition to *sym*-$N_2O_4$, there are two asymmetric $N_2O_4$ isomers, namely *trans*-$N_2O_4$ and *cis*-$N_2O_4$.[17–19] Zhu *et al.*[8] predicted the possible geometric conformations of $N_2O_4$ isomers based on *ab initio* molecular dynamics, and identified the most stable isomers as *sym*-$N_2O_4$ and *trans*-$N_2O_4$. Meanwhile, the spontaneous dissociation of $N_2O_4$ to $NO_2$ is less likely in the liquid propellant storage environment. Therefore, the work in this section mainly considers the mutual isomerization between *sym*-$N_2O_4$, *cis*-$N_2O_4$, and *trans*-$N_2O_4$. The potential energy surface (PES) and the geometric configurations and bond parameters of the conformers during the isomerization are shown in Fig. 1. The optimized *sym*-$N_2O_4$ has an N–N bond length of about 1.80 Å and N–O bond lengths of about 1.18 Å, in good agreement with reported values determined experimentally by electron diffraction analysis at 252 K.[20] When *sym*-$N_2O_4$ isomerizes to *cis*-$N_2O_4$, the N–N bond length in TS1 is 2.68 Å and the dihedral angle O4–N2–O6–N1 is 177°. The associated potential energy barrier is 166.91 kJ $mol^{-1}$, which further completes the isomerization process of $NO_2$ proposed by Liu *et al.*[3] In contrast, the "roaming-like" TS structure proposed by Putikam *et al.*[9] is more relaxed, with an N–N bond length of 3.70 Å, a dihedral angle O4–N2–O6–N1 of 76°, and a potential energy barrier of 34.31 kJ $mol^{-1}$, significantly different from the values calculated here. For the isomerization of *sym*-$N_2O_4$ to *trans*-$N_2O_4$ *via* TS3, the two $-NO_2$ groups of the reactants and products are coplanar, but the structure of TS3 is vertical, the N–N bond length is only 2.08 Å, and the associated potential energy barrier is about 175.94 kJ $mol^{-1}$. In contrast, in the TS structure reported in the literature, the N–N bond length reaches 3.57 Å, the two $-NO_2$ groups are almost dissociated, and the electron

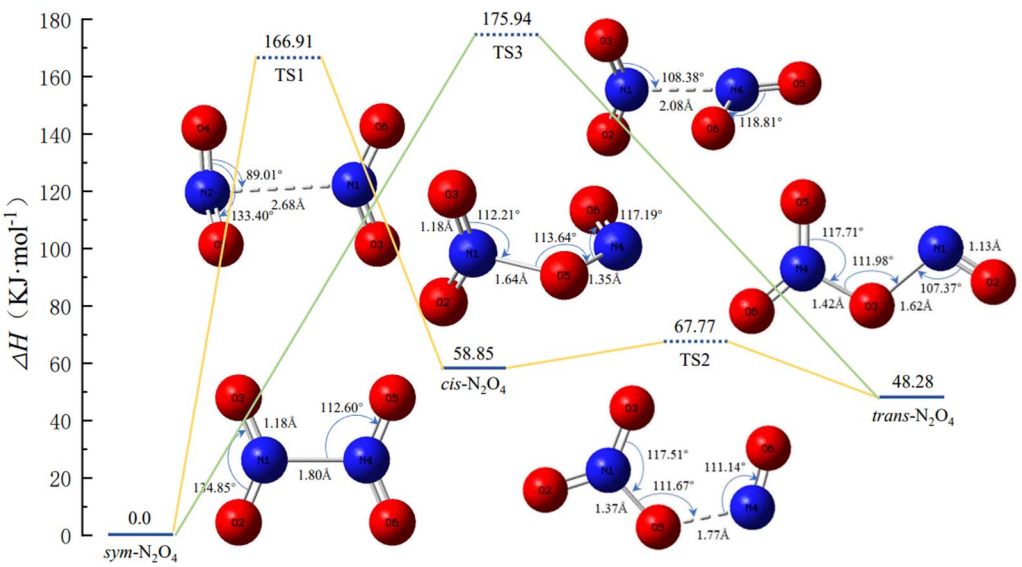


Fig. 1 Potential energy surface of $N_2O_4$ isomerization and the geometries and bond parameters of the conformers (key length unit: Å, key angle unit: °).

density between the interacting groups is reduced, so the TS potential energy barrier (53.56 kJ $mol^{-1}$) is much lower than that calculated here.[9] The course of the isomerization of *cis*-$N_2O_4$ to *trans*-$N_2O_4$ is similar to that calculated in the literature.[21]

### 3.2 Isomerization and reaction processes of $N_2O_4(H_2O)$ and $N_2O_4(H_2O)_2$ ($n$ = 1, 2)

From Section 3.1, it is clear that the relative energy of *trans*-$N_2O_4$ is lower than that of *cis*-$N_2O_4$, indicating that the former is more stable in the course of the isomerization. Hence, only *trans*-$N_2O_4$ is considered in the following calculations. Fig. 2 shows the PES and the geometric configurations of the molecules with bond parameters for the isomerization and reaction course of $N_2O_4(H_2O)$. When $N_2O_4$ absorbs $H_2O$, a complex such as IM1 is produced due to van der Waals forces. At this point, two pathways are available for IM1 for the next reaction step.

(1) IM1 may be directly converted to $HNO_3$ + *trans*-HONO *via* TS4, as shown in Fig. 2. TS4 is a compact five-membered-ring structure with an associated potential barrier of 138.62 kJ $mol^{-1}$. This value is similar to that reported by Chou *et al.*[22] Upon further conversion of TS4, H8 in $H_2O$ gradually detaches and combines with one of the $-NO_2$ groups to produce *trans*-HONO. The remaining –OH of $H_2O$ combines with the other $-NO_2$ group to produce $HNO_3$.

(2) IM1 may be converted to TS5 to generate *trans*-$ONONO_2$. In this case, the structure of TS5 is more similar to TS3. In the course of isomerization of *sym*-$N_2O_4$ to *trans*-$N_2O_4$, one of the $-NO_2$ groups rotates about the N–N bond, thus causing a shift of $H_2O$, and the distance between N1 and O7 reaches 4.02 Å. When structurally stable *trans*-$ONONO_2$ is generated, the distance between N1 and O7 is 2.85 Å. As the reaction continues, *trans*-$ONONO_2$ produces $HNO_3$ + *trans*-HONO and $HNO_3$ + *cis*-HONO through two six-membered-ring transition states, TS6 and TS7, respectively. In TS6, H8 of $H_2O$ is transferred to O5 in $-NO_3$, eventually forming $HNO_3$, while the remaining –OH of $H_2O$ combines with –NO. The structure of TS7 is similar to that of TS6, except that $H_2O$ is rotated by a certain angle. It follows a similar reaction course to finally form $HNO_3$ + *cis*-HONO, the reaction potential of which is 2.41 kJ $mol^{-1}$ higher than that of $HNO_3$ + *trans*-HONO.

In Fig. 2, it can be seen that the energy of *trans*-HONO is lower than that of *cis*-HONO, indicating that the former is more stable and the reaction pathway is more likely to occur. Therefore, the reaction course of *cis*-HONO is not considered in the following calculations. When the content of $H_2O$ is further increased, $N_2O_4$ combines with more $H_2O$ in the vicinity to produce $N_2O_4(H_2O)_2$. The PES and geometric configurations of the molecules with bond parameters for the isomerization and reaction course are shown in Fig. 3.

Similar to IM1 in Fig. 2, when $N_2O_4$ is combined with 2 $H_2O$, two $N_2O_4(H_2O)_2$ complexes, IM2 and IM3, are produced, as shown in Fig. 3(b), in which the 2 $H_2O$ molecules are located on the same or opposite sides of $N_2O_4$, respectively. Therefore, its reaction course will follow two main pathways.

**3.2.1 IM2 reaction process.** ① IM2 is directly converted to TS12, from which $HNO_3$ + *trans*-HONO + $H_2O$ are formed. TS12 has a five-membered-ring structure, similar to TS4, with only one $H_2O$ molecule involved in the reaction. Meanwhile, O10 of the other $H_2O$ molecule interacts with H8 and O7 in the five-membered-ring structure to form an O–H–O hydrogen bond.

② IM2 first passes through TS8 to form *trans*-$N_2O_4$–$2H_2O$. Both $H_2O$ molecules are involved in the reaction course, and the product *trans*-$N_2O_4$–$2H_2O$ has an eight-membered-ring structure. Upon further reaction of *trans*-$N_2O_4$–$2H_2O$, the final product is formed through TS10. During this process, both $H_2O$ molecules engage in proton-transfer phenomena, *i.e.*, O7 and

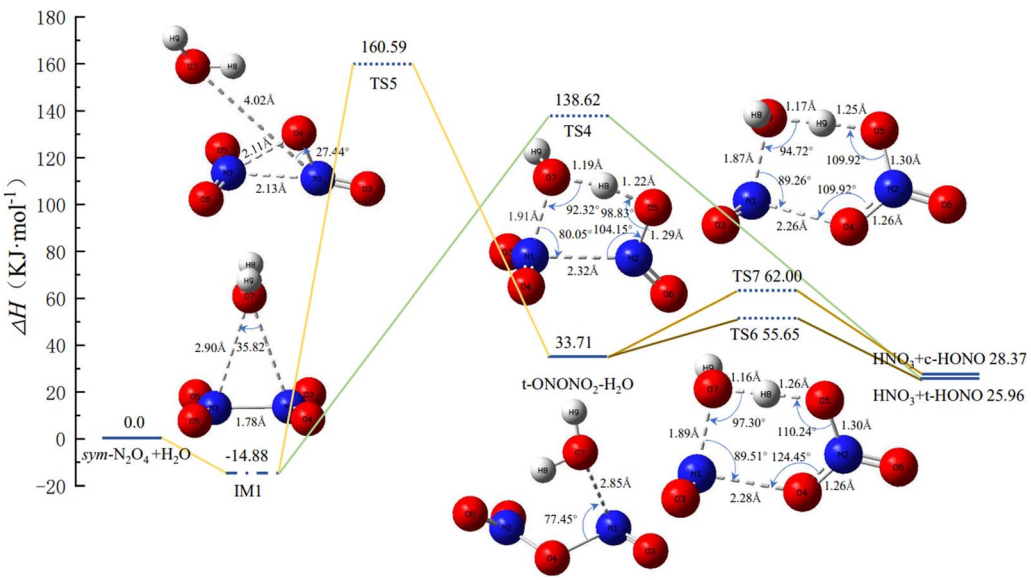


Fig. 2 Potential energy surface of $N_2O_4(H_2O)$ isomerization and reaction process, and the geometries and bond parameters of molecules (key length unit: Å, key angle unit: °).

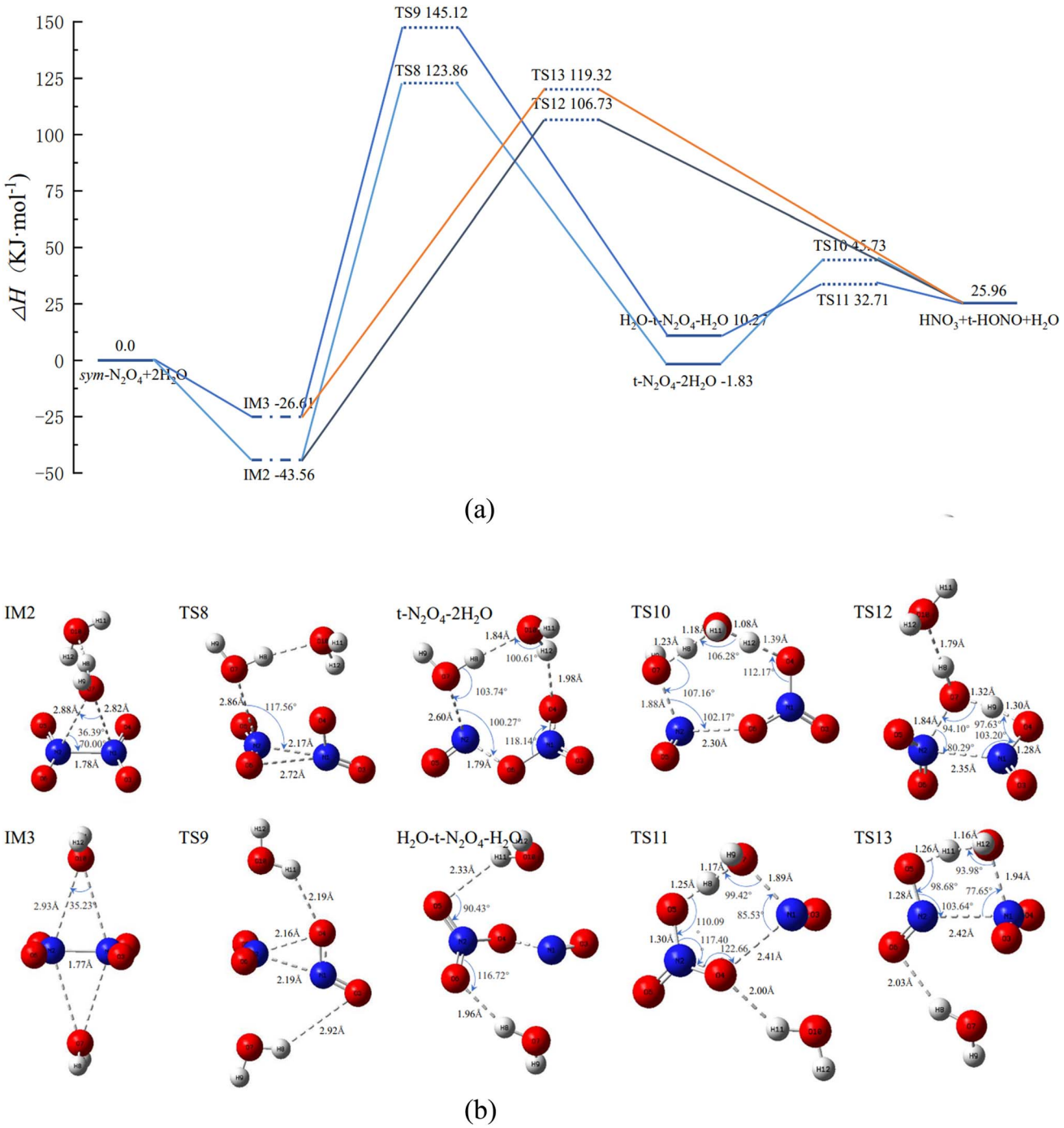


Fig. 3 (a) PES of $N_2O_4(H_2O)_2$ isomerization and reaction course. (b) Molecular geometrical configurations and bond parameters for $N_2O_4$–$(H_2O)_2$ isomerization and reaction course (bond lengths in Å, bond angles in °).

H10 of one $H_2O$ molecule combine with NO to form *trans*-HONO, while H12 of the other $H_2O$ molecule combines with $NO_3^-$ to form $HNO_3$. The remaining H8 and O10 of the two $H_2O$ molecules recombine with H11 to form a new $H_2O$ molecule.

**3.2.2 IM3 reaction process.** ① IM3 undergoes a direct reaction *via* TS13 to form $HNO_3$ + *trans*-HONO + $H_2O$. The two $H_2O$ molecules of IM3 in the steady state are symmetrically distributed on the upper and lower sides of $N_2O_4$, forming four N–O bonds, which are longer than the N–O bonds in IM2. Hence, IM3 is higher in energy than IM2. Upon isomerization of IM3, the $H_2O$ molecule on one side resides closer to $N_2O_4$ after rotating through a certain angle about the N–N bond, and can participate in the reaction. At this point, TS13 also adopts a five-membered-ring structure. Compared with TS12, only the atoms connected to $H_2O$ (O7), which is free from the five-membered-ring structure, are different. H9 of $H_2O$ (O7) in TS13 is connected to O6 of one of the $-NO_2$ groups, forming a stable TS structure.

② IM3 can also go through TS9 to first form $H_2O$–*trans*-$N_2O_4$–$H_2O$, and then O7 of $H_2O$, which is closer to N1, binds to N1 to form the six-membered-ring structure TS11. The latter is lower in energy and more stable than the eight-membered-ring structure of TS10. Of the $H_2O$ (O7) molecule involved in the reaction, H8 combines with $NO_3$ to form $HNO_3$, while O7 and H9 combine with NO to form *trans*-HONO.

### 3.3 Isomerization and reaction profile of $N_2O_4(H_2O)_3$ ($n = 3$)

In $N_2O_4(H_2O)_3$, there are two possible distributions of $H_2O$ molecules, *i.e.*, all three $H_2O$ molecules residing on one side of $N_2O_4$, or two $H_2O$ molecules on one side and the third on the other side. Our calculations reveal that $N_2O_4$–$3H_2O$ is lower in energy than $2H_2O$–$N_2O_4$–$H_2O$. Combined with the results in Section 3.2, $2H_2O$–$N_2O_4$–$H_2O$ can be studied with reference to the isomerization and reaction profiles of IM2 and IM3, and so this section focuses on the isomerization and reaction profiles of $N_2O_4$–$3H_2O$, for which the PES and the geometric configurations and bond parameters of the molecules are shown in Fig. 4.

(1) IM4 may directly generate $HNO_3$ + *trans*-HONO + $2H_2O$ *via* TS16. In IM4, the three $H_2O$ molecules are connected sequentially to form a ring structure with one of the $-NO_2$ groups, while O10 of the $H_2O$ molecule located above $N_2O_4$ forms a stable triangular structure with both N atoms. The two N–O bonds are almost equal in length. Although only one $H_2O$ molecule is involved in the reaction, $H_2O$ (O10), in TS16 it forms both an eight-membered-ring structure with the remaining two $H_2O$ molecules and a five-membered-ring structure with $N_2O_4$.

(2) IM4 first forms *trans*-$N_2O_4$–$3H_2O$ *via* TS14, and the three $H_2O$ molecules also break from the ring structure into a single chain and then rejoin with O3 to form a ring. The *trans*-$N_2O_4$–$3H_2O$ then undergoes proton transfer, with $H_2O$ (O7) providing –OH and $H_2O$ (O10) providing H to form IM5. IM5 already has the structure of the products, but the molecules are still connected to each other and only form the products after bond-breaking.

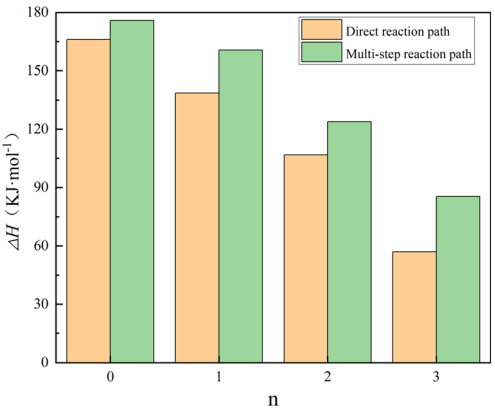


Fig. 5 Potential energy barriers associated with different reaction paths for $N_2O_4(H_2O)_n$ isomerization reactions.

$N_2O_4(H_2O)_n$ has one and only one stable structure during the isomerization and reaction course when $n < 2$. When $n \geq 2$, the distribution of $H_2O$ affects the stable structure of $N_2O_4(H_2O)_n$, resulting in different energies. If $H_2O$ is distributed on the same side of $N_2O_4$, with fewer interconnected chemical bonds and shorter bond lengths, the energy is lower and the structure is more stable, as in IM2 and IM3 in Fig. 3(b). Irrespective of whether $n$ is odd or even, multiple pathways are available for $N_2O_4(H_2O)_n$ to undergo isomerization reactions. To verify the speculation of Miller *et al.*,[4] the potential energy barriers associated with different pathways of $N_2O_4(H_2O)_n$ isomerization for different values of $n$ and pertaining to the most stable conformation are plotted in Fig. 5.

The energy of 166.01 kJ $mol^{-1}$ for $n = 0$, *i.e.*, the direct ionization of $N_2O_4$ to form NO + $NO_3$, and combining TS4, TS12, and TS16 as the reaction potential for the direct reaction of $N_2O_4(H_2O)_n$ to form the product pathway; the first step of isomerization process of $N_2O_4(H_2O)_n$ through multiple steps to generate products as the reaction potential of its multi-step reaction pathway, *i.e.*, $N_2O_4(H_2O)_n \rightarrow$ *trans*-$N_2O_4$–$(H_2O)_n$: TS3, TS5, TS8, and TS14. From Fig. 5, it can be seen that the potential

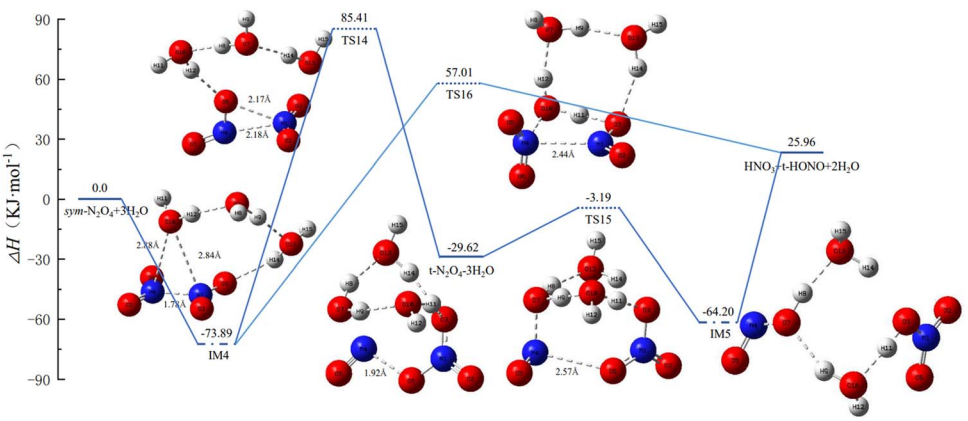


Fig. 4 Potential energy surface of $N_2O_4(H_2O)_3$ isomerization and reaction process, and the geometries and bond parameters of molecules (key length unit: Å, key angle unit: °).

Table 1 Variations in charge on the *trans*-$ONONO_2$ group and ON–$ONO_2$ bond length in *trans*-$ONONO_2$–$(H_2O)_n$

| $n$ | 0 | 1 | 2 | 3 |
|---|---|---|---|---|
| Electric charge/a.u. | 0 | −0.019 | −0.025 | −0.503 |
| Key length/Å | 1.62 | 1.76 | 1.79 | 2.57 |

energy barrier of $N_2O_4(H_2O)_n$ gradually decreases as $n$ is increased and more $H_2O$ is involved in the reaction. When $n$ = 0–2, the differences in the potential energy barriers associated with the direct and multi-step reaction paths are small, such that $N_2O_4(H_2O)_n$ may follow both reaction paths at the same time. When $n = 3$, however, the difference in potential energy barriers associated with the two paths reaches 28.4 kJ $mol^{-1}$, indicating that $N_2O_4(H_2O)_3$ will preferentially pass through TS16 to afford the products directly. Combined with the finding in Fig. 4 that TS15 is lower in energy than the reaction potential of the products when $N_2O_4(H_2O)_3$ undergoes a multi-step reaction path, it is clear that the multi-step reaction path of $N_2O_4$–$(H_2O)_3$ is difficult to reach. On the basis of thermodynamics, Mulliken charge analysis was performed on the intermediate product *trans*-$ONONO_2$–$(H_2O)_n$, and the results in terms of charge on the *trans*-$ONONO_2$ group and ON–$ONO_2$ bond length are shown in Table 1.

As can be seen from Table 1, the charge on the *trans*-$ONONO_2$ group gradually becomes more negative as the $H_2O$ content in *trans*-$ONONO_2$–$(H_2O)_n$ is increased, indicating increased polarity. Concomitantly, the bond length of ON–$ONO_2$ also increases, and –ON gradually dissociates and from the *trans*-$ONONO_2$ group. It can be seen that the differences in charge on the *trans*-$ONONO_2$ group and ON–$ONO_2$ bond length are not large when $n = 1$ and 2. However, when $n = 3$, the charge on the *trans*-$ONONO_2$ group and the ON–$ONO_2$ bond length change abruptly, reaching −0.503 a.u. and 2.57 Å, respectively. These results support the conjecture of Miller *et al.*;[4] when $n = 1$ or 2, *trans*-$ONONO_2$-$(H_2O)_n$ is partly ionically bonded, but still mainly covalently bonded. When $n = 3$, however, ionic bonding becomes dominant. Meanwhile, combined with the reaction rate results of Miller *et al.*[4] and analyzed by the potential energy surfaces in Fig. 2–4, the reaction rate constant increases by two orders of magnitude when $n = 3$ compared with $n < 3$. In Section 3.2.1, *trans*-$N_2O_4$–$2H_2O$ was seen to undergo a proton-transfer phenomenon as the reaction proceeds. Luo *et al.*[14] confirmed that the formation of hydrogen bonds and a polar environment are prerequisites for intermolecular proton transfer. Proton-transfer due to *trans*-$ONONO_2$ dominates in the production of –OH, which is also supported by experimental results,[23] leading to a shorter lifetime of *trans*-$ONONO_2$ with the increase of $H_2O$. All charge-transfer steps result in partial reverse charge-transfer from $NO_3^-$ to $NO^+$, making the ON–$ONO_2$ bond less susceptible to cleavage, further verifying that when $n = 3$, the $N_2O_4(H_2O)_3$ system is dominated by ionic bonds between molecules. Due to the short-lived existence of *trans*-$ONONO_2$ and the difficulty of breaking the ON–$ONO_2$ bond, the reaction can be considered as being completed instantaneously.[24] That is to say, IM4 mainly passes through TS16 to directly generate the final products $HNO_3$ + *trans*-HONO + $2H_2O$.

# 4 Conclusions

(1) $N_2O_4(H_2O)_n$ system structure reaction course of the local minimum is not related to the parity of the $n$ value. When $H_2O$ molecules are distributed on the same side, the potential energy of the system is lower, and the structure is more stable. When $n$ = 1 or 2, the two reaction pathways are similar in energy. The systems are partly ionically bonded, but mainly still covalently bonded.

(2) When $n = 3$, the charge on the *trans*-$ONONO_2$ group and the ON–$ONO_2$ bond length change abruptly, reaching −0.503 a.u. and 2.57 Å, respectively, and the system is then dominated by ionic bonds.

(3) When $n = 2$, the reaction course shows the phenomenon of proton-transfer, with partial reverse charge-transfer from $NO_3^-$ to $NO^+$, making cleavage of the ON–$ONO_2$ bond more difficult. Combining the change of potential energy surface, the charge on the $ONONO_2$ group, and the molecular bond parameters during the course of the reaction, it is again verified that $N_2O_4(H_2O)_n$ tends to afford the products directly in one step with increasing $H_2O$ content in the system.

# Author contributions

Y. Guo: conceptualization, investigation, methodology, writing – original draft. Z. Y. Huang: data curation, formal analysis. G. Tian: project administration, validation. W. Wu: resources, supervision. J. Lin: software, validation. X. L. Chang: funding acquisition, writing – review & editing.

# Conflicts of interest

We declare that we do not have any commercial or associative interest that represents a conflict of interest in connection with the work.

# Acknowledgements

This research was funded by the National Natural Science Foundation of China (No. 52272446) and Natural Science Foundation of Shaanxi Province (No. 2021JM-250).

# References

1 Y. Guo, X. L. Chang, G. Tian, D. J. Liu and C. Pang, *Rare Met. Mater. Eng.*, 2022, **51**, 3459–3465.
2 D. J. Liu, G. Tian, Z. W. Yang, G. F. Jin, W. Zhang, Y. Wang and H. L. Wei, *Chin. J. Aeronaut.*, 2022, **36**, 304–315.
3 W. G. Liu and A. G. William, *J. Am. Chem. Soc.*, 2012, **134**, 12970–12978.
4 Y. Miller, B. J. Finlayson-Pitts and R. B. Gerber, *J. Am. Chem. Soc.*, 2009, **131**, 12180–12185.
5 A. S. Pimentel, C. A. L. Francisco and A. B. F. da Silva, *J. Phys. Chem. A*, 2007, **111**, 2913–2920.

6 D. J. Medeiros and A. S. Pimentel, *J. Phys. Chem. A*, 2011, **115**, 6357–6365.
7 I. I. Zakharov, *Theor. Exp. Chem.*, 2012, **48**, 233–239.
8 R. S. Zhu, K. Y. Lai and M. C. Lin, *J. Phys. Chem. A*, 2012, **116**, 4466–4472.
9 R. Putikam and M. C. Lin, *Int. J. Quantum Chem.*, 2017, **118**, 25560–25569.
10 B. J. Finlayson-Pitts, L. M. Wingen, A. L. Sumner, D. Syomin and K. A. Ramazan, *Phys. Chem. Chem. Phys.*, 2003, **5**, 223.
11 T. C. Marilia, J. M. Anglada, J. S. Francisco and M. F. Ruiz-Lopez, *J. Am. Chem. Soc.*, 2020, **142**, 20937–20941.
12 F. Menezes and G. M. Popowicz, *Phys. Chem.*, 2022, **23**, 395.
13 Y. Miller and R. B. Gerber, *Phys. Chem. Chem. Phys.*, 2008, **10**, 1091–1093.
14 G. F. Luo and X. B. Chen, *J. Phys. Chem. Lett.*, 2012, **3**, 1147–1153.
15 J. S. Zhao, Z. Y. Huang, G. F. Jin, M. N. Gao and H. X. Zhu, *Chin. J. Energ. Mater.*, 2021, **29**, 1125–1131.
16 M. J. Frisch, G. W. Trucks, H. B. Schlegel, G. E. Scuseria, M. A. Robb, J. R. Cheeseman, G. Scalmani, V. Barone, G. A. Petersson, H. Nakatsuji, X. Li, M. Caricato, A. V. Marenich, J. Bloino, B. G. Janesko, R. Gomperts, B. Mennucci, H. P. Hratchian, J. V. Ortiz, A. F. Izmaylov, J. L. Sonnenberg, D. Williams-Young, F. Ding, F. Lipparini, F. Egidi, J. Goings, B. Peng, A. Petrone, T. Henderson, D. Ranasinghe, V. G. Zakrzewski, J. Gao, N. Rega, G. Zheng, W. Liang, M. Hada, M. Ehara, K. Toyota, R. Fukuda, J. Hasegawa, M. Ishida, T. Nakajima, Y. Honda, O. Kitao, H. Nakai, T. Vreven, K. Throssell, J. A. Montgomery Jr, J. E. Peralta, F. Ogliaro, M. J. Bearpark, J. J. Heyd, E. N. Brothers, K. N. Kudin, V. N. Staroverov, T. A. Keith, R. Kobayashi, J. Normand, K. Raghavachari, A. P. Rendell, J. C. Burant, S. S. Iyengar, J. Tomasi, M. Cossi, J. M. Millam, M. Klene, C. Adamo, R. Cammi, J. W. Ochterski, R. L. Martin, K. Morokuma, O. Farkas, J. B. Foresman, and D. J. Fox, *Gaussian 16, Revision A.03*, Gaussian, Inc., Wallingford CT, 2016.
17 A. Givan and A. Loewenschuss, *J. Chem. Phys.*, 1989, **90**, 6135.
18 A. Givan and A. Loewenschuss, *J. Chem. Phys.*, 1989, **91**, 5126.
19 A. Givan and A. Loewenschuss, *J. Chem. Phys.*, 1991, **94**, 7562.
20 B. W. McClelland, G. Gundersen and K. Hedlberg, *J. Chem. Phys.*, 1972, **56**, 4541.
21 K. Y. Lai, MS thesis, National Chiao Tung University, Taiwan, 2009.
22 A. Chou, R. Zhi and F. M. Tao, *J. Phys. Chem. A*, 1999, **103**, 7848.
23 T. Kinugawa, S. Enami, A. Yabushita, M. Kawasaki, M. Hoffmann and A. Colussi, *Phys. Chem. Chem. Phys.*, 2011, **13**, 5144–5149.
24 A. Yabushita, S. Enami, Y. Sakamoto and M. Kawasaki, *J. Phys. Chem. A*, 2009, **113**, 4844–4848.